Constraints on the cosmological density of compact objects from gravitational microlensing of quasars

Carina Persson

Master thesis
Supervisor: Erik Zackrisson

June 1, 2003

Abstract

New improved constraints on Ω_C, the cosmological density of compact objects relative the critical density, have been calculated using the gravitational microlensing effect. Compact objects with masses between $\sim 10^{-3}$ and $\sim 40\, M_\odot$ will amplify the continuum emission of quasars without changing the line emission and thus the emission line equivalent width is reduced. By comparing models of the expected increase of small equivalent width objects with observations, Ω_C is constrained to be < 0.05 for compact objects in the mass range $0.01 - 1\, M_\odot$ for a source size equal or less than 10^{13} m, $\Omega_C < 0.1$ for compact objects with $0.01 - 2\, M_\odot$, $\Omega_C < 0.2$ for compact objects with $0.001 - 8\, M_\odot$ and $\Omega_C < 0.3$ for compact objects with $0.001 - 40\, M_\odot$. This has been done by implementing the small equivalent width method (used by Dalcanton et al, 1994) in Matlab and generalizing from an Einstein-de Sitter Universe to a Λ-dominated cosmology. This will increase the optical depth for which a new expression is derived and calculated. Uncertainties in source size and size of the broad line emission region have also been taken into account. This determines new upper and lower mass limits of the compact objects.

Contents

1 Introduction

The Universe is thought to be made up by dark matter and dark energy (only $\sim 0.5\%$ is visible), but their nature and distribution is unknown. The dark matter could exist in the form of weakly interacting massive particles or as compact astrophysical objects. How can we learn more about dark matter and is it possible to detect? Yes, it can be done with gravitational lensing. This is the result of the bending of light rays by gravitational fields and it is sensitive to both luminous and dark matter alike.

If the lenses are very massive the deflection is strong and several images of the source can be seen. This is called macrolensing, the multiple imaging of a source. If the lenses are small and not strong enough to form two distinct images of a background source it may still magnify its brightness to an observable extent. This is called microlensing and is one of the most promising ways known to detect small compact objects.

These compact objects can be a part of a galaxy or they can be cosmologically distributed and filling intergalactic space.

Since compact objects can lead to a magnification of distant sources and since sources and lenses are moving, the magnification will change with time. The observed time scale for the lensing event can be used to give the most probable lens mass. Searches for lensing events by compact objects in the Galactic halo has been done by monitoring millions of stars in the Magellanic Clouds (EROS and MACHO projects). Results of Alcock et al (2000) indicated that the most likely mass of the compact objects (interpreted as a Galactic halo population) is between 0.15 and 0.9 $M_{\odot}$. The greatest achievements of these projects though has been to rule out most forms of compact dark matter as the dominant contributors to the dark halo. Results from Afonso et al (2003) yields strong limits. Less than 25% of a typical halo model can be composed of objects with a mass between $2 \cdot 10^{-7} - 1 M_{\odot}$ at the 95 % confidence level. But, it is possible that the observed microlensing events comes entirely from an undetected foreground or background population in the outer galaxy or in the Magellanic Clouds. Since very few microlensing events have been detected (and some of them probably are due to self-lensing) the results so far point to the fact that the observed microlensing events are caused by stars within the Magellanic Clouds, and that the contribution of compact objects to dark matter in our halo is 0-5 % (Kailash C Sahn, 2003).

The MACHO and EROS projects are based on the assumptions that the compact objects are uniformly distributed and bound to the galactic halo. Clustering effects of the compact objects are also neglected. Constraints on the cosmological density of the compact objects cannot be obtained, only in fractions of the dark matter of the Galactic halo. Furthermore, the searches for gravitational microlensing of stars in the Magellanic Clouds are sensitive only to strong gravitational lenses, that is compact objects with high column densities ($> 10^4 g\ cm^{-2}$). They would not detect cold gas clouds with $10^2 g\ cm^{-2}$, so the limits inferred from the MACHO and EROS projects do not apply to them (Walker and Wardle, 1999).

If the compact objects are cosmologically distributed and not bound to galaxies, investigation of the equivalent width distribution of quasar emission lines can set upper limits on the cosmological density of compact objects (Canizares, 1982; Dalcanton et al, 1994). This method is based upon the fact that compact objects (in a wide mass range) can magnify the brightness of the small continuum emitting region (CR) in quasars, while the broad line emitting region (BLR) will be little affected due to its larger radius. The continuum is thus magnified by the microlensing event, but the magnification of the line emission is unaltered. This will make the equivalent width of the emission lines from the BLR much smaller. The higher the density of compact objects and the larger the redshift to the quasar, the more apparent will this effect be. If a flux-limited sample of quasars at low redshift is compared to a sample at high redshift, then the latter should have a higher fraction of small equivalent widths objects. By comparing models of the equivalent width distribution with observations the cosmological density of compact objects can therefore be constrained. At these large distances even the diffuse gas clouds would appear compact, because their size would be smaller than their Einstein-radius (see section 2.1).

Dalcanton et al (1994, hereafter D94) investigated this and since the expected increase of small equivalent width quasars was not found they concluded that Ω_C, the cosmological density of

compact objects relative to the critical density (see section 2.1), must be < 0.1 in the mass range $0.01 - 20M_{\odot}$ for $\Omega_{total} \lesssim 0.6$ (see section 2.1), $\Omega_C < 0.2$ for compact objects with $0.001 - 60M_{\odot}$ and $\Omega_C < 1$ for compact objects with $0.001 - 300M_{\odot}$ irrespective of Ω_{total}.

The article of D94 is often referred to when ruling out any significant cosmological density of compact objects. Carr (2000) refers to their limits of Ω_C and so do Wambsganss (2002), Coles & Lucchin (2002) among others. Since the method and their constraints on Ω_C are one of the most powerful today it is important to revisit this with new data available today, which is the purpose of this work.

The issues in D94 that needs to be reexamined is the cosmology and the effects of new BLR and CR sizes. The cosmology used by D94 is a flat Einstein-de Sitter universe (section 2.1). Generalizing this to a Lambda-dominated universe *increases* the probability of lensing compared to an Einstein-de-Sitter universe.

For simplicity D94 assumed that the total density of all matter is equal to Ω_C and only estimated the constraints when $\Omega_C \neq \Omega_M$. This point needs further investigation.

Recent research indicate that the BLR could be substantially smaller than expected in the standard model used by D94 and this affects the *upper* limits of the lens masses that this test can constrain.

The CR size affects the *lower* mass-limits of the compact objects. In D94 a standard size of the CR was assumed, but since the geometry and size of the CR is highly uncertain the impact of different sizes is examined.

The luminosity function used by D94 is from Boyle et al (1990) and needs to be substituted. This will affect the amplification bias.

These issues are examined by implementing the D94 method in matlab. A code listing is given in Appendix A.

In section 2 basic cosmology, lensing theory and the theory of statistical microlensing for a point source are developed. Then the effects of a finite source size, the BLR size and the amplification bias are taken into account and finally the predicted distribution of equivalent widths of quasar emission lines is calculated. Section 3 describes the general considerations when choosing a quasar sample and the sample used here. In section 4 the predicted distribution is compared to the observations and in section 5 the results are presented. Section 6 contains a discussion of possible uncertainties, comparison of the results of D94 and the future of microlensing in this field. A summary is given in section 7.

2 Theory of magnification distributions

2.1 Basic cosmology

It was Edwin Hubble in 1929 that proved that the Universe is expanding. The Hubble parameter $H(t)$ measures the expansion rate of the Universe.

There are three different possible geometries for the Universe: closed, flat and open. The critical density of matter (corresponding to a flat Universe) distinguishes between the closed and open cases and is defined as:

$$\rho_{critical} = \frac{3H^2(t)}{8\pi G} \tag{1}$$

where $H(t)$ is the Hubble parameter and G is the gravitational constant.

The average density of matter relative the critical density is defined as a dimensionless matter density parameter:

$$\Omega_M = \frac{\rho_M}{\rho_{critical}} \tag{2}$$

and the dimensionless compact objects parameter similarly as:

$$\Omega_C = \frac{\rho_C}{\rho_{critical}} \, . \tag{3}$$

A flat matter-dominated Universe is called an Einstein-de Sitter Universe and the total dimensionless matter density in this Universe is:

$$\Omega_{total} = \Omega_M = 2q_0 \tag{4}$$

where q_0 is a deceleration parameter (measures the rate by which the Universe is slowing down).

Recent results from WMAP (Spergel, 2003) shows that $\Omega_{total} = 1.02 \pm 0.02$ and $\Omega_M = 0.27^{+0.04}_{-0.04}$. Approximately 73% of the energy content in the Universe is assumed to consist of vacuum energy (or dark energy). It is defined as:

$$\Omega_\Lambda = \frac{\rho_V}{\rho_{critical}} = \frac{\lambda/8\pi G c^2}{\rho_{critical}} \, . \tag{5}$$

Here λ is a cosmological constant (introduced by Einstein) and corresponds to a tiny but universal force acting on matter. This constant was assumed to be zero only a few years ago. A Universe with a non-zero cosmological constant is called a Λ-dominated Universe if $\Omega_\Lambda > \Omega_M$.

In this Universe $\Omega_{total} = \Omega_M + \Omega_\Lambda$. Ω_M and Ω_C can consist of ordinary baryonic dark matter or non-baryonic dark matter.

The nature of the compact objects are not known but there are many suggestions. Among those are: primordial black holes, white dwarfs, brown dwarfs, neutron stars, stellar black holes and cold H_2 gas clouds.

Whenever applying a Λ-dominated cosmology $\Omega_\Lambda = 0.70$, $\Omega_M = 0.30$ and the WMAP value of $H_0 = 71 \, kms^{-1}Mpc^{-1}$ (Spergel, 2003) will be used.

2.2 Lensing theory

Any mass distribution located between the source and the observer will lead to an magnification of the luminosity. Since the deflection angle is proportional to the lens mass one of the applications of gravitational lensing is the determination of the mass of the deflector.

If a light ray passes close to a point mass within a distance l_0 (the impact parameter, see fig. 1 and section 2.3), then it feels an acceleration component perpendicular to its direction of motion.

The resulting deflection angle α is then (as predicted by general relativity):

$$\alpha = \frac{4GM_C}{l_0 c^2} \tag{6}$$

provided that α is small. Here M_C represents the lens mass of a compact object, G is the gravitational constant and c is the speed of light.

The simplest situation in which a mass can be determined is that of a spherical deflector with a source right behind the centre of the lens and a ring shaped image (the Einstein ring) will be seen. This is shown in fig. 1.

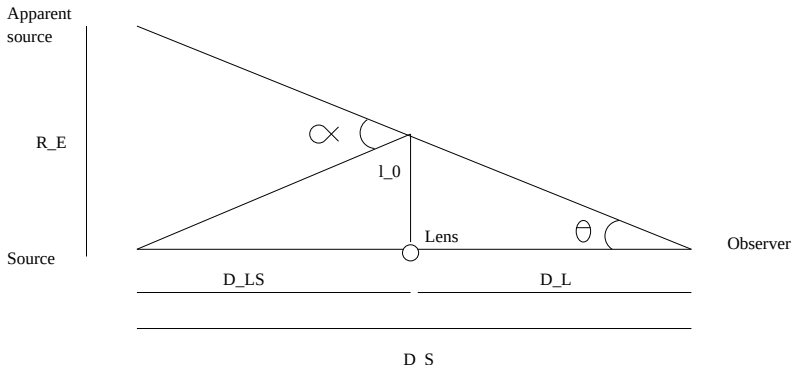

Figure 1: The geometry of a lensing event.

The subscrips LS, L and S refers to distances from the lens to the source, from the observer to the lens and from the observer to the source respectively.

The relevant length scale for microlensing is the Einstein radius in the source plane and is defined (Schneider et al, 1991) as:

$$R_E = \sqrt{\frac{4GM_C}{c^2}\frac{D_S D_{LS}}{D_L}} \approx 4 \cdot 10^{12} \sqrt{\frac{M_C}{M_\odot}}\ m \tag{7}$$

where the typical redshift of a typical lens is at $z_L \approx 0.5$ and with a source at redshift $z_{source} \approx 2$ (Wambsganss, 2000). D is the angular diameter distance.

This length scale translates into an angular scale of the Einstein angular radius (fig. 1):

$$\theta_E = \frac{R_E}{D_S} \approx 10^{-6} \sqrt{\frac{M_C}{M_\odot}}\ arcsec\,. \tag{8}$$

Small lens objects are not detectable by multiple imaging as the image separation lies in the range $19 \cdot 10^{-5} - 10^{-6}\sqrt{(\frac{M}{M_\odot})}$ arcsec if the source is a distant quasar. For microlensing in the Milky Way the Einstein angle is of the order of milliarcsec (Wambsganss, 2000). This gives only a magnification of the luminosity and no observable splitting of the source image.

For an object to be compact it has to have a size of its Einstein radius or smaller.

Due to the relative motion of the lens, observer and source, the total magnification will change with time. The duration of the brightening depends on the mass and velocity of the lens, and the geometry of the event.

2.3 Magnification probability for point sources

This section describes the theory of statistical lensing for a point source with an lensing model developed by Canizares (1982) (built upon Press & Gunn, 1973 and Weinberg, 1976) and used by D94. It will give an approximate but analytically simple form for the probability of lensing. The effect of a finite source size is taken into account in section 2.6.

The lenses are assumed to be distributed uniformly, with constant comoving density (and each one can act as a gravitational lens). The probability distribution depends on the lens population in the universe, as well as on the redshift and source size.

If the universe is considered to be isotropic and homogeneous (the cosmological principle) the Robertson-Walker metric can be used to derive a relation of cosmological distance measure to redshift from the field-equations of general relativity. But the universe is not homogeneous on scales smaller than galaxy clusters. The inhomogeneities will affect the measured distances through gravitational lensing and it is not possible to obtain exact solutions for this model. Instead simple methods can be used to compute approximate distances such as the Dyer & Roeder (1972) distance-redshift relation in a universe in which all matter is concentrated into objects such as galaxies. If a beam of light propagates far away from these objects it is approximately as if the beam propagates along a small empty tube in an otherwise homogeneous universe. The effects of gravitational lensing by the clumps of matter is handled by putting point masses back into the cone and analyze the scattering events.

The effects of clumping of lenses is neglected because correlations between them are not important. Correlations are only important for clumps that contain a sizable fraction of the matter along a given line of sight. But such dense clumps are not expected, not even in the most extreme models of large-scale structure (D94).

The Dyer & Roeder (1972) empty cone distance:

$$D(z) = \frac{c}{H_o}\lambda(z) \tag{9}$$

where $\lambda(z)$ is the affine parameter (Dyer & Roeder, 1972):

$$\lambda(z) = \int_0^z (1+z')^{-3}(1+2q_0z')^{-1/2}\,dz' \,. \tag{10}$$

In this expression the cosmological constant is assumed to be zero. The optical depth is defined to be the mean number of lenses that fall within the impact parameter l_0. Objects whose lines of sight pass within l_0 of the lens will be magnified by a factor greater than μ_0 which is chosen to be 1.061 (the magnification when the bending angle equals the critical angel $\alpha_0 = 2\cdot\theta_E$). The magnification $\mu = L_{obs}/L_{intrinsic}$ is always larger than 1.

The impact parameter l_0 (fig. 1) can be expressed as:

$$l_0^2(z';z) = 16\frac{M_C G}{cH_0}(1+z')\frac{\lambda(z')}{\lambda(z)}[\lambda(z)-\lambda(z')] \,. \tag{11}$$

The probability $p_u(\mu_u, z'; z)\,d\mu_u\,dz'$ that an object at redshift z obtaining a magnification from μ_u to $\mu_u + d\mu_u$ from a single lens within redshift $z' + dz'$ factors into two independent probabilities $p_z(z';z)\,dz'$ and $p_1(\mu_u)\,d\mu_u$:

$$p_u(\mu_u, z'; z)\,d\mu_u\,dz' = p_z(z';z)\,p_1(\mu_u)\,d\mu_u\,dz' \,. \tag{12}$$

$p_z(z';z)$ denotes the probability of finding a lens at z' within l_0, and $p_1(\mu_u)$ is the probability of one lens producing a magnification.

$$p_z(z';z)\,dz' = \frac{(1+z')^2}{\sqrt{1+2q_o}}\frac{\lambda(z')}{\lambda(z)}[\lambda(z)-\lambda(z')]\,dz' \,, \tag{13}$$

$$p_1(\mu_u)\,d\mu_u = \begin{cases} \frac{1}{2.015}\,(\mu_u^2-1)^{-3/2}\,d\mu_u & : \quad \mu_u \geqslant \mu_0 \,, \\ 0 & : \quad \mu_u < \mu_0 \,, \end{cases} \tag{14}$$

The subscript u is used to denote that the probability of magnification is uncorrected for flux conservation (see section 2.4). $p_z(z';z)$ can be integrated to find the optical depth for a source at redshift z:

$$N_C(z) = \int_0^z p_z(z';z)\,dz' \,. \tag{15}$$

If the optical depth $N_C(z) \geqslant 1$ contributions from two or more lenses, $p_2(\mu_u)$, must be considered. It is found by convolving two single lens probabilities with the assumption that one lens is weak and that the net amplification equals the product of two individual magnifications:

$$p_{\geqslant}2(\mu_u)\, d\mu_u = \begin{cases} 2.525\ \mu_u^{-3}\, d\mu_u & : \quad \mu_u \geqslant \mu_0^2\,, \\ 0 & : \quad \mu_u < \mu_0^2\,. \end{cases} \tag{16}$$

In addition if no point masses are near the line of sight within l_0 through an inhomogeneous universe, the quasar light is dimmed relative to that in a homogeneous universe and $p_0(\mu_u)$ must be added. This is the empty cone case:

$$p_0(\mu_u; z)\, d\mu_u = \delta(\mu_u - 1) \tag{17}$$

where $\delta(\mu_u - 1)$ is a delta function centered at $\mu_u = 1$.

For magnifications less than μ_0 and μ_o^2 respectively $p_1(\mu_u)$ and $p_2(\mu_u)$ are defined to be zero. (The minimum magnification of $p_2(\mu_u)$ is the product of the minimum magnification of two lenses.)

The optical depth is used to calculate the Poisson probabilities of having 0, 1 or $\geqslant 2$ lenses along the line of sight. $P_0 = e^{-N_C}$, $P_1 = N_C e^{-N_c}$, $P_2 = 1 - P_0 - P_1$.

$p_1(\mu_u)$ and $p_2(\mu_u)$ are both normalized to unity. $p_0(\mu_u; z)$ is already by the definition of a delta function normalized to unity.

$$\int_{\mu_0}^{\infty} p_1(\mu_u)\, d\mu_u = 1, \qquad \int_{\mu_0^2}^{\infty} p_2(\mu_u)\, d\mu_u = 1. \tag{18}$$

The probability of lensing can now be approximated as:

$$p_u(\mu_u; z) = P_0(z)p_0(\mu_u) + P_1(z)p_1(\mu_u) + P_{\geqslant 2}(z)p_{\geqslant 2}(\mu_u). \tag{19}$$

These three terms corresponds to having none, one and two or more lenses within l_0.

2.4 Flux conservation

Light bending must not violate the law of flux conservation. If the total flux of energy through any surface surrounding a given object is considered, it is obviously independent of whether the matter inside that surface is distributed smoothly or in clumps. The *mean* flux density is therefore that expected in a homogeneous universe in which the lens material is spread out uniformly (Peacock, 1982; Canizares, 1982; D94). The magnification considered is thus the magnification relative to the case where the lens mass were absent. Lens masses lying outside the cone described by $l_0(z'; z)$ will defocus the light in the cone and cause a diminution of the image (D94; Canizares, 1982). The demagnifications are necessary to balance the magnifications from strong lensing events so that (20) is satisfied.

To compensate for this $p_u(\mu_u; z)$ is scaled to smaller magnifications μ by a constant diminution factor μ_z, such that $\mu = \mu_z \mu_u$, and is chosen to satisfy the constraint of flux conservation (D94; Canizares, 1982):

$$< \mu >= \int_0^{\infty} \mu p(\mu; z) d\mu = 1. \tag{20}$$

This implies $\mu_z = \frac{1}{<\mu_u>}$ where

$$< \mu_u >= \int_0^{\infty} \mu_u p_u(\mu_u; z) d\mu_u. \tag{21}$$

With this correction the final expression for $p(\mu; z)$ then becomes (D94; Canizares, 1982):

$$p(\mu; z) =< \mu_u > [P_0(z)p_0(\mu_u) + P_1(z)p_1(\mu_u) + P_{\geqslant 2}(z)p_{\geqslant 2}(\mu_u)]. \tag{22}$$

This is an approximation and a conservative way of determining Ω_C because it tends to underestimate the true amount of lensing (D94). Note that the expression for $p(\mu; z)$ contains no dependence

on the mass of the lensing compact objects. All the information about Ω_C is contained in the Poisson probabilities (which is calculated from the optical depth).

2.5 A new optical depth with non-zero cosmological constant

Generalizing from a Einstein-de Sitter Universe to a Λ-dominated Universe will affect the optical depth through an increased path length. Another expression for the affine parameter (10) with a non-zero cosmological constant is needed.

The affine parameter-redshift differential equation is (Seitz, Schneider, Ehlers, 1994):

$$\frac{dz}{d\lambda} = \frac{1}{c}\frac{\frac{d}{dt}R(t)}{R(t)}[1+z(\lambda)]^2 = \frac{1}{c}\frac{\frac{d}{dt}R(t)}{R(t_0)}[1+z(\lambda)]^3 \tag{23}$$

where R(t) is the scale factor.

This equation can be solved and gives (Schneider, 1997):

$$\lambda(z) = \int_0^z \frac{c}{H_0}\frac{dz'}{(1+z')^3\sqrt{1+z'\Omega_M - \Omega_\Lambda(1-(1+z')^{-2})}} \,. \tag{24}$$

With $\Omega_C = \Omega_M$ and $\Omega_\Lambda = 0$ this expression is equal to (10).

The microlensing optical depth is just the lenses in a "tube" from the observer to the source. It is independent of the velocities of the lenses and sources and independent of the lens masses. The only dependence is on the lens density distribution. Assume that the lenses are conserved, i.e. the number density of lenses is $n_C = n_{0,C}(1+z)^3$, where $n_{0,C}$ is the present value of n_C and that all compact objects have the same mass. It is related to the cosmological parameters by:

$$n_{0,C} = \Omega_C \frac{3H_0^2}{8\pi G M_C} \,. \tag{25}$$

The differential number of lenses along the line of sight is:

$$dN_C = n_C dV = n_{0,C}(1+z')^3 dV \,. \tag{26}$$

A circular cross-section is considered which radius is the Einstein radius. The volume element is $A \cdot dD_{proper}$ where the area is (with l_0 from equation (11)):

$$A = \pi l_o^2 = \frac{\pi 16 M_C G}{cH_0}(1+z')\frac{\lambda(z')}{\lambda(z)}[\lambda(z) - \lambda(z')] \,. \tag{27}$$

Differentiate equation (9) to get the differential distance and use the relationship $dD_{proper} = (1+z')d\lambda$ (Seitz, Schneider & Ehlers, 1994). This will give a new expression for the optical depth along the line of sight with a non-zero cosmological constant:

$$\begin{aligned} N_C &= \int_0^z dN_C \\ &= 6\Omega_C \int_0^z \frac{(1+z')^2}{\sqrt{1+z'\Omega_M - \Omega_\Lambda(1-(1+z')^{-2})}} \frac{\lambda(z')}{\lambda(z)}[\lambda(z) - \lambda(z')] \,. \end{aligned} \tag{28}$$

With $\Omega_\Lambda = 0$ and $\Omega_M = \Omega_C$ this expression is equal to (15).

Fig. 2 shows the optical depth as a function of redshift. In this figure different values of Ω_C is plotted, as well as with different cosmologies.

In a Ω_Λ-dominated universe *the increased path length increases the optical depth.* Compare $\Omega_C = 0.2$ and $\Omega_C = 0.1$ for the different cosmologies in fig.2. This will *increase* the probability of lensing and *decrease* the resulting Monte Carlo probabilities (i.e. stronger constraints can be set).

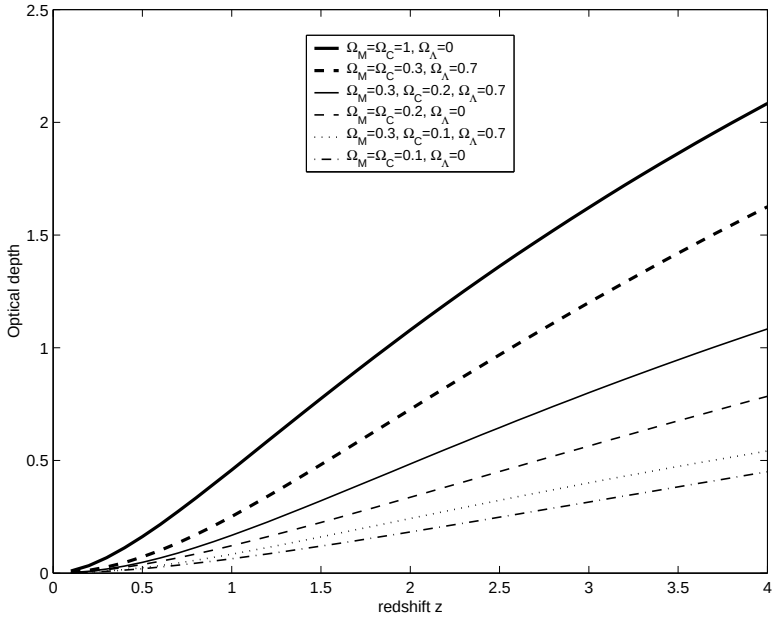

Figure 2: The optical depth as a function of redshift.

2.6 Finite source size

It is believed that the central regions driving the activity of quasars and active galatic nuclei (AGNs) is an accretion disc surrounding a supermassive black hole. As gases fall onto the black hole, their gravitational energy is converted into radiation. In the standard model the size of the UV-optical continuum CR is at least a few times the gravitational radius (Collin et al 2001), which for a 10^{8-9} $M_\odot$ black hole is $1.5 \cdot 10^{11-12}$ m. Since the expected angular size of accretion discs is too small to be resolved spatially, quasar microlensing can be used to obtain information of the central regions. The strongest hint for very small source sizes comes from variability, but the geometry of the CR is complicated and mainly unknown.

If most quasars do have large CRs then no constraints can be placed on the small lens masses because for these even the compact CR will behave like an extended source. How large is the CR allowed to be then before it will appear extended and what size of the CR should be used in this test?

By following the detection of a gravitational microlensing event in Q2237+0305A, Wyithe et al (2000) determined the CR size and found that the most likely size is $2 \cdot 10^{12}$ m. Upper and lower limits of the R-band continuum is $6 \cdot 10^{13}$ m and $2 \cdot 10^{11}$ m respectively (99% confidence level). They also considered the joint probability for source size and mean lens mass and found that the mean lens mass lies between ~ 0.01 and ~ 1 $M_\odot$ (95% confidence). (These results are depending on an estimated event duration of 52 days for the high magnification event.)

For the same quasar Shalyapin et al (2002) derived new information of the size. They inferred that 90% of the V-band and R-band luminosities are emitted from a region with radial size less than $3.7 \cdot 10^{14}$ m (2 σ confidence level). For a uniform disc $R_V = 1.9 \cdot 10^{13}$ m (at 1σ confidence).

For the Double Quasar QSO 0957+561 A,B, Refsdal et al (2000) found an upper limit of $6 \cdot 10^{13}$ m at a significance level of 10 %.

The most commonly used CR size is 10^{13} m (in D94 the CR size is assumed to be $0.0003\,pc \approx 9.3 \cdot 10^{12}\,m$). Because of the uncertainty of source size, the sizes considered here is $10^{12} - 10^{14}$ m.

If the source cannot be considered as a point source, there is a maximum possible magnification μ_{max} (D94):

$$\mu_{max} = \sqrt{1 + \left(\frac{l_0^{proj}}{l_{source}} \right)^2} \tag{29}$$

where l_0^{proj} is l_0 from the lens plane to the source plane. In the statistical lensing approach this is substituted with $< l_0^{proj} >_{z'}$, which is the average of l_0^{proj} over z', weighted by $p_z(z';z)$ (D94):

$$< l_0^{proj} >_{z'} = \frac{\int_0^z l_0(z';z)\, p_z(z';z) dz'}{\int_0^z p_z(z';z) dz'}. \tag{30}$$

With the new expression for $p_z(z';z)$ this gives:

$$< l_0^{proj} >_{z'} = \frac{24\Omega_C}{N_C(z)} \sqrt{\frac{M_C G}{cH_0}} \int_0^z \frac{(1+z')^{5/2}}{\sqrt{1+z'\Omega_M - \Omega_\Lambda[1-(1+z')^{-2}]}} \left(\frac{\lambda(z')}{\lambda(z)} \right)^{3/2} [\lambda(z) - \lambda(z')]^{3/2} dz. \tag{31}$$

(Note misprint in D94 equation without Ω_Λ.)

The maximum magnification possible then becomes (D94):

$$\mu_{max} = \sqrt{1 + \frac{g^2(z) M_C}{l_{source}^2}} \tag{32}$$

where $g(z) =< l_0^{proj} >_{z'} / M^{1/2}$. This function is little dependent of z_{source} or Ω_C and is not affected much by introducing a new cosmology. This is because in equation (31) the fraction $\Omega_C / N_C(z)$ remains constant (≈ 0.41) when Ω_C is varied. $g(z)$ varies a little around 0.43 and depends only weakly on H_0 (an inverse correlation exists between μ_{max} and H_0). The dependence of μ_{max} of the lens mass M_C and the source size l_s is shown in figure 2.

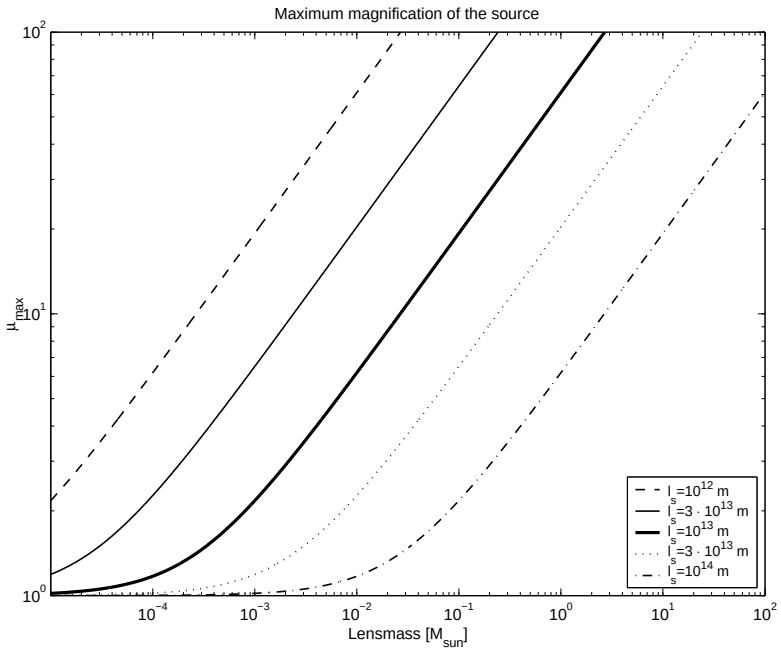

Figure 3: Maximum magnification as a function of lens mass for different source sizes: $l_s = 10^{12}$ m (dashed), $l_s = 3 \cdot 10^{12}$ m (thin solid), $l_s = 10^{13}$ m (thick solid), $l_s = 3 \cdot 10^{13}$ m (dotted), $l_s = 10^{14}$ m (dash-dotted); z=2, $\Omega_M = \Omega_C = 0.3$, $\Omega_\Lambda = 0.7$ for all l_s.

If the lens mass is small and the source size is larger than or equal to $< l_0^{proj} >_{z'}$, so that $\mu_\mu^{max} \approx 1$, equation (22) is no longer correct. The total intensity of the source must be averaged

over many lines of sight from the influence of several compact objects at different redshift. Since this is not trivial, $p(\mu; z)$ is constrained by flux conservation (20) and normalization:

$$\int_0^\infty p(\mu; z)\, d\mu = 1\,. \tag{33}$$

With these two constraints Canizares (1982) and D94 solves the problem by approximating the rapid roll-off in the probability distributions $p_1(\mu_u)$ and $p_{\geqslant 2}(\mu_u)$ by cutting them off att $\mu_u = \mu_{max}$. A delta function is added at the cutoff which preserves the normalization. Here this is done for $p_1(\mu_u)$, but not for $p_2(\mu_u)$. If the minimum magnification is μ_0^2 (the product of the minimum magnification of two lenses) then the maximum magnification should be the product of the maximum magnification of *two* lenses! (Is this another misprint in D94?) Here the delta function that preserves the normalization for $p_2(\mu)$ is added at $\mu_u = \mu_{max}^2$.

$$p_1(\mu_u)d\mu_u = B\delta(\mu_u - \mu_u^{max})d\mu_u \qquad \mu_u \geqslant \mu_u^{max} \tag{34}$$

$$p_2(\mu_u)d\mu_u = C\delta(\mu_u - (\mu_u^{max})^2)d\mu_u \qquad \mu_u \geqslant (\mu_u^{max})^2 \tag{35}$$

B and C is computed by normalizing $p_1(\mu_u)$ and $p_2(\mu_u)$ to unity.

This is a simple way of taking a finite source size in account. (Schneider et al, 1992 found another perhaps more correct approximation of a finite source size.)

For a given source size a specific μ_{max} thus corresponds to a certain lens mass. If the source size is varied a constant μ_{max} corresponds to different lens masses and can be calculated if equation (32) is solved for the lens mass and $g(z)$ is known from equation (31).

In table 1 corresponding μ_{max} and lens masses are listed for different source sizes. This is approximate values (with z=2.0 and $h = 0.71$), since they differ slightly with redshift and source size. In the resulting table with Monte Carlo results (section 5.3) μ_{max} corresponding to lens masses have been calculated for different source sizes.

Table 1: Approximate values of μ_{max} corresponding to different lens masses for different source sizes.

	$l_s = 10^{12}$m	$l_s = 3 \cdot 10^{12}$m	$l_s = 10^{13}$m	$l_s = 3 \cdot 10^{13}$m	$l_s = 10^{14}$ m
μ^{max}	$M_C\ [M_\odot]$	$M_C\ [M_\odot]$	$M_C\ [M_\odot]$	$M_C\ [M_\odot]$	$M_C\ [M_\odot]$
1.2	10^{-6}	10^{-5}	10^{-4}	10^{-3}	10^{-2}
2.2	10^{-5}	10^{-4}	10^{-3}	10^{-2}	10^{-1}
6.2	10^{-4}	10^{-3}	10^{-2}	10^{-1}	1
19.3	10^{-3}	10^{-2}	10^{-1}	1	10
61	10^{-2}	10^{-1}	1	10	100
193	0.1	1	10	100	1000

2.7 Amplification bias

An object not intrinsically bright enough to be included in a flux-limited sample can still be detected if it is magnified sufficiently by lensing. The fraction of lensed objects in the sample will then be greater than otherwise expected. This effect is called amplification bias and may have an influence on source counts and the luminosity function.

The effect of the amplification bias depends very strongly on the form and slope of the quasar luminosity function. If the luminosity function is steep, there are many more faint sources available to be lensed into the sample than there are for a shallow power law (D94; Canizares, 1982). One of the indications for the importance of amplification bias is the apparent number excess of galaxies around high-redshift QSOs found by several groups (D94).

There are different opinions on the importance of amplification bias. One is that practically all bright quasars are highly magnified if Ω_C is large enough, the lens mass is larger then $0.01 M_\odot$ and the CR is small. (Schneider, 1992; Bartlemann and Schneider, 1990). Others considers this view simplistic and suggest that amplification bias is not so strong (Wyithe and Turner, 2002). Here D94 and Canizares (1982) are followed.

The observed numbers of sources in the luminosity interval (L, L+dL) is (Canizares, 1982; Schneider,1987):

$$n_{obs}(L)\, dL \propto \int_1^\infty \frac{d\mu}{\mu} p(\mu) n\left(\frac{L}{\mu}\right) dL \tag{36}$$

where n is the number density of quasars . The flux conservation and normalization of $p(\mu; z)$ imply that the index of a power-law luminosity function is unchanged by lensing (Canizares, 1982). With a power law $n = n_0 L^{-\alpha}$ this gives (Canizares, 1982; Schneider, 1987):

$$n_{obs} dL \propto \int_1^\infty p(\mu)\, \mu^{\alpha-1} d\mu\, dL\,. \tag{37}$$

Here a broken power-law form for the luminosity function is assumed. For the slope of the steep and shallow power laws, α and β are used. R is the ratio of the flux limit of the sample to the flux at the break in the luminosity function. (Calculation of R in section 2.8.) The corrected $p(\mu; z)$ becomes (D94):

$$p_s(\mu; z) = \frac{p(\mu; z)}{N} * \begin{cases} \left(\frac{\mu}{R}\right)^{\alpha-1} & : \quad \mu < R \\ \frac{\alpha-1}{\beta-1}\left[\left(\frac{\mu}{R}\right)^{\beta-1} - 1\right] + 1 & : \quad \mu \geqslant R \end{cases} \tag{38}$$

where N is a normalization factor. This correction of $p(\mu; z)$ assumes $R \geq 1$. If $R < 1$ only the second case of (38) applies.

The amplification bias is strongly dependent on R and α. If $R < 1$ then only quasars from the shallow end of the luminosity function will be available to be lensed into the sample and the amplification bias will be much weaker than if $R > 1$.

For moderate magnifications $p_s(\mu; z) \propto \mu^{-(4-\alpha)}$ which decreases more slowly than $p(\mu; z) \propto \mu^{-3}$ ($\alpha > 1$). With $\alpha = 3.41$ from Boyle et al (2000), $p(\mu; z) \propto \mu^{-0.59}$. For larger magnifications ($\mu \geq R$) the effect is not so strong (the amplification bias is then dependent on β). With $\beta = 1.41$ from Boyle et al (2000) $p(\mu; z) \propto \mu^{-2.59}$.

This is the final corrected expression for the probability that an object at redshift z obtaining a magnification μ. The probability for lensing from (19) has now been corrected for flux conservation, a finite source size and the effect of amplification bias.

2.8 Calculation of the strength of the amplification bias

With α given from the luminosity function it is R that can change the strength of the amplification bias.

R is calculated using:

$$R = \frac{L_{limit,sample}}{L^*(z)} = 10^{0.4[M^*(z) - M_{B,sample}(z)]} \tag{39}$$

where $L^*(z)$ ($M^*(z)$) is the luminosity (absolute magnitude) at the break of the luminosity function.

To obtain $< R >_{median}$, $< z >_{median}$ is used.

To obtain a strong amplification bias a sample where the luminosity is brighter than the break luminosity at the medium redshift of the subsample is needed.

If the apparent magnitude is known then the absolute magnitudes can be calculated with (Kayser et al, 1997):

$$M = m - 5log\left(\frac{D_L[pc]}{10[pc]}\right) - K \tag{40}$$

where K is the correction term defined as $K = 2.5(\alpha - 1)log(1+z)$, $\alpha = 0.5$, and D_L is the luminosity distance in pc. This term takes into account the fact that the observed wavelength interval is redshifted compared to the corresponding interval of emission. Less radiation is observed because the bandwidth at the observer is $(1+z)$ times larger than the source, if the spectrum is flat. If it's not, additional corrections must be included based on the shape of the spectrum. A power-law continuum for the quasars is assumed with slope $\alpha = 0.5$.

The new luminosity function has been taken from Boyle et al (2000). The break of the magnitude in this luminosity function is best described by a second-order polynomial function (and not as previously with a power-law evolutionary model):

$$M_B^*(z) = M_B^*(0) - 2.5(k_1 z + k_2 z^2) \tag{41}$$

where $k_1 = 1.36, k_2 = -0.27$ and $M_B^*(0) = -22.65$ are adopted from Boyle et al (2000) assuming $\Omega_M = 0.3$ and $\Omega_\Lambda = 0.7$. The slope of the luminosity function has also changed from $\alpha = 3.97$ and $\beta = 1.41$ (Boyle, 1990) to $\alpha = 3.41$ and $\beta = 1.58$ (Boyle, 2000).

The effect of the new function for the break magnitude of the luminosity function, a weaker strength of the amplification bias and a less steep slope of the luminosity function is a *weaker* bias than that assumed in D94. If the sample used by D94 is also used here, the resulting Monte Carlo probabilities will *decrease* (i.e. weaker constraints on Ω_C can be set). If a brighter sample is used where the limiting magnitude is several magnitudes brighter than the luminosity function break, then the constraints on Ω_C would be stronger.

2.9 Mass range of compact objects

2.9.1 Upper mass limits of compact objects

If the mass of the compact objects is high enough to magnify not only the CR but also the BLR, then the small equivalent width method cannot be used. Recent research indicate that the BLR could be substantially smaller than expected in the standard model, which assumed the BLR to have radius in the 0.1 - 1 pc range ($\approx 3 \cdot 10^{15-16}$ m; Wandel et al, 1999; Collin et al, 2001). If the BLR is smaller, this will decrease the upper mass limits of the compact objects that can be constrained.

The most commonly accepted model of the BLR consists of an assembly of photoionized clouds (Collin et al, 2001). A major tool for examine the structure of the BLR is reverberation mapping, through the study of correlated variations of the lines and continuum fluxes. For low-luminosity AGNs (mainly Seyfert galaxies) Wandel et al (1999) inferred a size in the range of a few lt-days to a few lt-weeks ($\approx 10^{13} - 9 \cdot 10^{14}$ m). For 17 Palomar-Green QSOs Kaspi et al (2000) derived sizes from the Balmer lines in the range from 39 to 319 lt-days ($10^{15} - 10^{16}$ m). They also found a global scaling of the BLR size as a function of the 5100 Å luminosity, $r_{BLR} \propto L^{0.7\pm0.03}$.

The scatter in BLR sizes can be attributed to the different size/structure of the BLR in different objects and different sizes of the regions associated with emission lines of different degrees of ionization.

The question is if there exist lensed quasars with BLR radius smaller than the projected Einstein radius of the microlens on the source? Abajas et al (2002) investigated this (using a flat cosmology, $\Omega_M = 0.3$, $h = 0.7$ and the Kaspi relationship $r_{BLR} \propto L^{0.7\pm0.03}$). Their conclusion were that the high-luminosity quasars should have no strong microlensing in the emission lines of BLR, if the lenses are star-sized objects. But for a z=2 quasar with $m_V = 22.5$ microlensing on the BLR would be quite pronounced. Since the sample from Steidel & Sargent (1991, see section 3.2.1) used in this investigation (and by D94) is bright it should not be a problem with lensed BLR if the lens mass is not higher than a star-sized object. But how high then are the lens masses allowed to be before the BLR will be lensed?

The test used to constrain Ω_C (described in section 4) compares the fraction of very small equivalent widths in a sample of quasars, $W_\lambda < W_{limit}$, to the fraction predicted by the model. The small equivalent widths have been magnified by a factor $\mu > \mu_{limit}$ (typically $\mu_{limit} \approx 2$). If the magnification of the BLR is neglected then the fraction of small equivalent width objects will be proportional to (D94):

$$f \propto \int_{\mu_{limit}}^{\infty} p_s(\mu; z) d\mu \, . \tag{42}$$

If the *line* is magnified by a factor of μ_{BLR} the number of objects in the small equivalent region will be *reduced* by a factor of $\Delta f/f$:

$$\frac{\Delta f}{f} = \frac{\int_{\mu_{limit}}^{\mu_{limit} \cdot \mu_{BLR}} p_s(\mu; z) \, d\mu}{\int_{\mu_{limit}}^{\infty} p_s(\mu; z) d\mu} \, . \tag{43}$$

Approximating $p_s(\mu; z) \propto \mu^{-2}$ (includes some correction for amplification bias) gives (D94):

$$\frac{\Delta f}{f} = \left(\frac{\mu_{BLR} - 1}{\mu_{BLR}} \right) \, . \tag{44}$$

With this approximation μ_{limit} cancels out.

The more lenses along the line of sight the larger the fraction of small equivalent widths. So if Ω_C is large, $\Delta f/f$ can be larger and still leave a detectable signal. Therefore the upper end of the mass range over which the equivalent width test is effective increases with Ω_C.

Here $\Delta f/f$ is allowed to be $\leqslant 0.15$, 0.25, 0.50, 0.75 for $\Omega_C = 0.05$, 0.10, 0.20 and 0.30 respectively. The corresponding upper limits on lens masses are 1, 2, 8 and 40 $M_\odot$ if the BLR size is 10^{15} m. (See section 5.3 for further discussion.)

2.9.2 Lower mass limits for compact objects

The lowest lens mass (corresponding to a certain μ_{max}) that this test can be used to constrain depends on the source size (see section 2.6), Ω_c, the redshift of the sample (through the optical depth) and the number of objects in the high-redshift sample. If the total number of objects is high then the resulting Monte Carlo probabilities will be low if the observed distributions are statistically identical.

If the lens mass is very small then the maximum magnification of the continuum μ_{max} is too small to take the object into the small equivalent region. Then this test cannot be used. D94 have a cutoff for lens masses less than $0.001 - 0.01 M_\odot$. But this is calculated with the assumption of a source size of $\approx 9.3 \cdot 10^{12}$ m. If the source size is smaller then the minimum mass for lenses that this test can constrain is lowered, if it is larger the minimum lens mass increases (see table 1 and section 5.4 for further discussion).

2.10 Emission line equivalent width distribution

The definition of equivalent width of an emission line λ_0 is:

$$W_\lambda = \int \frac{\Delta I_\nu}{I_\nu(\lambda_0)} d\lambda \, . \tag{45}$$

If the CR of a quasar is magnified by a compact object with a factor μ and the BLR is not, then the observed intensity of the continuum is increased to $\mu I_\nu(\lambda_0)$ while the intensity of the line ΔI_ν is effectively unchanged. $I_\nu(\lambda_0)$ is the intensity of the continuum under the line.

The *observed* equivalent width for a lensed object will then be *smaller* than for an unlensed object (D94):

$$W_\lambda = \frac{W_0}{\mu} \, . \tag{46}$$

Here W_0 represents the equivalent width that would be measured if the quasar were not lensed.

If $p_0(W_0)$ is the intrinsic distribution of equivalent widths and with $p_s(\mu; z)$ from (38), then the apparent distribution $p_W(W_\lambda)$ is (D94):

$$p_W(W_\lambda) = \int_0^\infty \mu \, p_s(\mu; z) \, p_0(\mu W_\lambda) \, d\mu \, . \tag{47}$$

The unlensed distribution can be represented as a log normal function (the distribution of W if lnW is Gaussian distributed; D94).

$$p_0(W_0) \, dW_0 = \frac{1}{\sqrt{2\pi\gamma^2}} e^{-[lnW_0 - \omega]^2/2\gamma^2} \frac{dW_0}{W_0} \, . \tag{48}$$

(Note three misprints in D94 in this equation.)

The resulting probability distribution of equivalent widths is shown in fig. 4-9 and shows how the distribution changes with redshift, Ω_C and maximum magnification μ_{max}. In fig. 4 and 5 the distributions of equivalent widths with $\Omega_C = 0.3$ and $\mu_{max} = 20$ is shown for a series of redshift. Note the rapid buildup of a tail at small equivalent widths. The small decrease of large equivalent widths are due to the diminution of the apparent brightness (see section 2.4). Fig. 6 and 7 shows the distribution of equivalent widths with z=2 and $\mu_{max} = 20$ for different Ω_C.

Note that fig. 4 and 6, fig. 5 and 7 almost have identical distributions. Approximately the same distribution is obtained for $\Omega_C = 0.05$, z=2 and $\Omega_C = 0.3$, z=0.5. Similarly $\Omega_C = 0.1$, z=2 are almost identical to $\Omega_C = 0.3$, z=1 and $\Omega_C = 0.2$, z=2 with $\Omega_C = 0.3$, z=1.5. If a high-redshift sample is used strong constraints on small Ω_C can be obtained.

In fig. 8 and 9 the distribution of equivalent widths with z=2 and $\Omega_C = 0.2$ is shown for different $\mu_{max} = 2.2$, 6.2 and 19.3. If $\mu_{max} \gtrsim 7$ then the maximum magnification of the CR is large enough that the resulting equivalent width distribution is almost completely independent of M_C. The reason for this is that $p_s(\mu; z)$ in (47) decreases very rapidly towards zero for high μ.

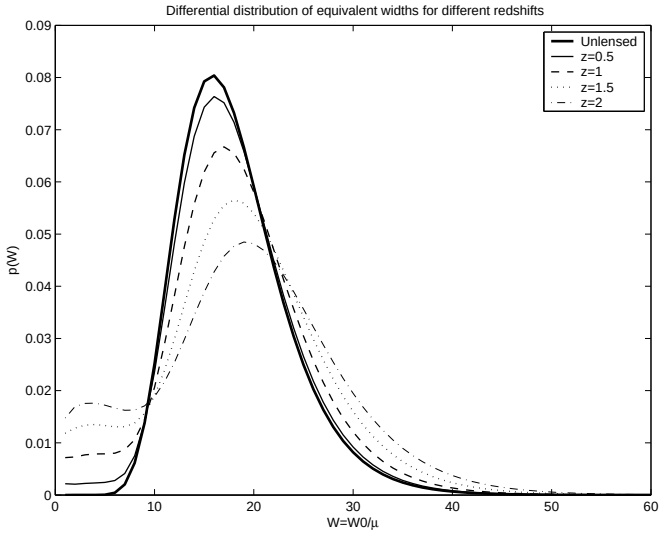

Figure 4: Differential distribution of equivalent widths for different redshift: z=0 (thick solid), z=0.5 (thin solid), z=1 (dashed), z=1.5 (dotted), z=2 (dash-dotted). $\Omega_C = \Omega_M = 0.3$, $\Omega_\Lambda = 0.7$, $\alpha = 3.41$, $\beta = 1.58$, R=1.6, $\gamma = 0.3$, $\omega = 2.85$ and $\mu_{max} = 20$ for all z.

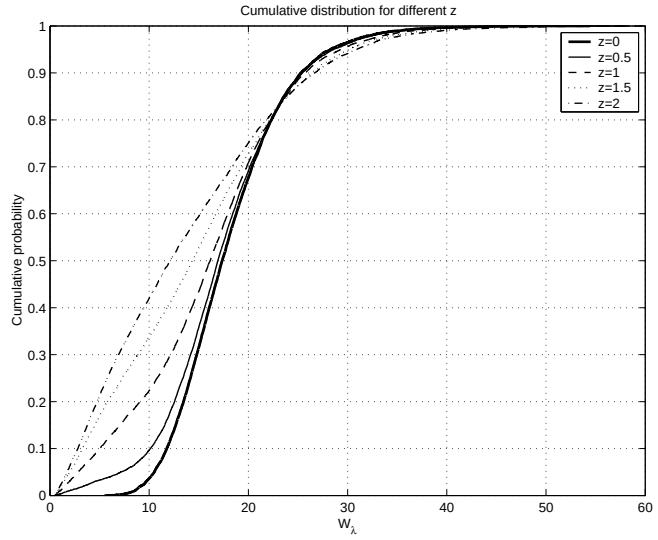

Figure 5: Cumulative probability distribution of equivalent widths for distributions with different z (parameters as in figure 4).

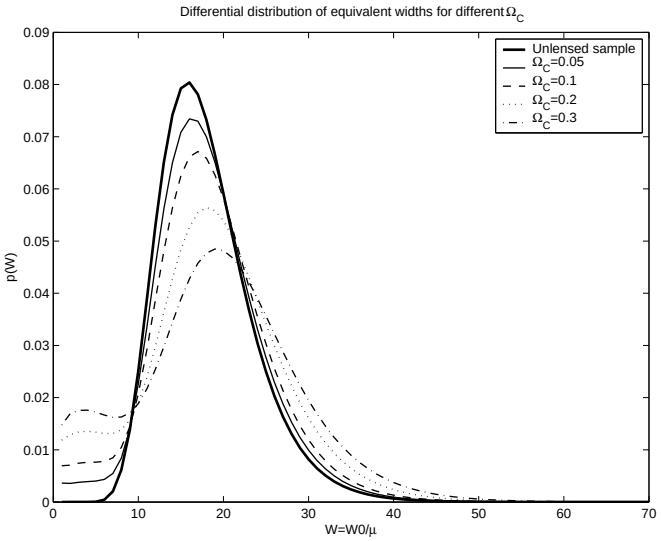

Figure 6: Differential distribution of equivalent widths for different Ω_C with redshift z=2 and $\mu_{max} = 20$: unlensed distribution (thick solid), $\Omega_c = 0.05$ (thin solid), $\Omega_C = 0.1$ (dashed), $\Omega_C = 0.2$ (dotted), $\Omega_C = 0.3$ (dash-dotted). R=1.6, $\gamma = 0.3$, $\omega = 2.85$, and $\alpha = 3.41$, $\beta = 1.58$, $\Omega_\Lambda = 0.7$ and $\Omega_M = 0.3$ for all Ω_C.

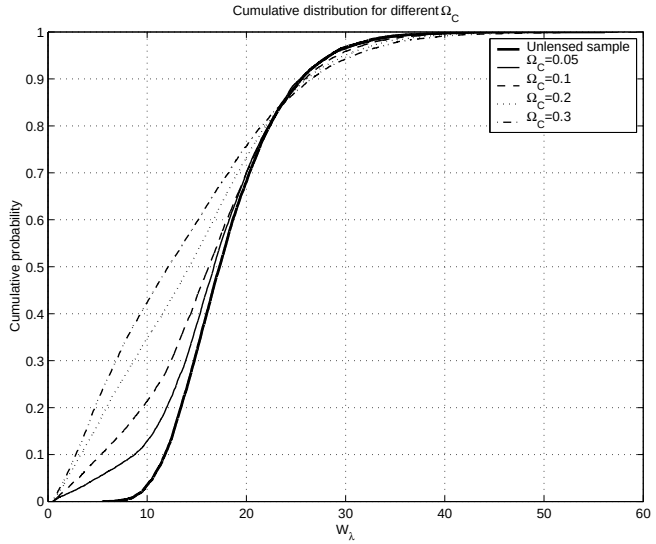

Figure 7: Cumulative distribution of equivalent widths for distributions with different Ω_C (parameters as i fig. 6).

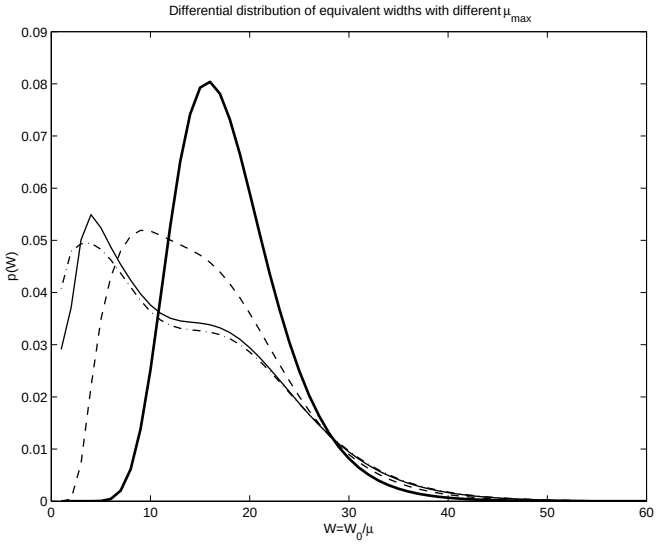

Figure 8: Differential distribution of equivalent widths for different μ_{max} with redshift z=2 and $\Omega_C = 0.3$: unlensed distribution (thick solid), $\mu_{max} = 2.2$ (dashed), $\mu_{max} = 6.2$ (thin solid) and $\mu_{max} = 19.3$ (dash-dotted). $\Omega_M = 0.3$, $\Omega_\Lambda = 0.7$, $\alpha = 3.41$, $\beta = 1.58$, R=1.6, $\gamma = 0.3$, $\omega = 2.85$ for all μ_{max}.

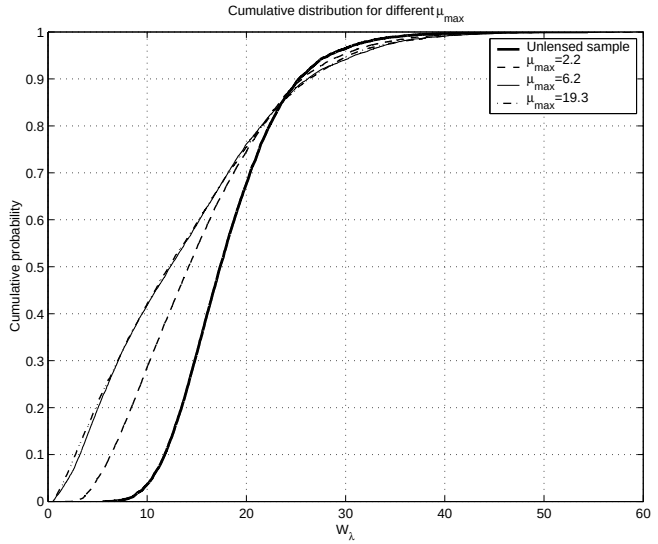

Figure 9: Cumulative distribution of equivalent widths for distributions with different μ_{max} (parameters as in fig. 8).

3 Observations

3.1 Considerations in choice of sample and emission lines

When choosing a sample to which the equivalent width test can be applied there are important aspects to consider.

- The time scales of the microlensing events

  The time lag between the selection of the quasars in the sample and the time when they were observed spectroscopically is important. If this is too long then the microlensing event that may have caused a quasar to be lensed into the sample will have ended. The equivalent widths of the quasar emission lines will have become uncorrelated with the presence of the quasar in the sample, and the amplification bias will be removed.

  If the compact objects is distributed randomly a typical time scale for a $\mu = 3$ microlensing event to fade to a $\mu = 1.7$ event to motion of the lens (D94):

  $$\Delta t_{microlens} \approx 82 \left(\frac{100 kms^{-1}}{v_{rel}} \right) \left(\frac{M}{M_\odot} \right)^{1/2} \quad yr \tag{49}$$

  where v_{rel} is the velocity of the lens relative to the line of sight from earth to the quasar. With a high velocity the time scale will be short. With $v_{rel} = 500\ kms^{-1}$ and a lens mass of $0.001\, M_\odot$ the time scale is approximately 0.5 yr. With $M = 0.01\, M_\odot$ and $v_{rel} = 200\ kms^{-1}$, $\Delta t \approx 4.1$ yr.

- Bias against weak lines

  The sample should not be biased against weak-lined quasars, which could be a possible problem for quasars identified on the basis of their line emission. If the objects are selected through UV excess there should be no bias. A complete quasar sample is of course ideal. D94 prefers X-ray selected samples because they should be unbiased in equivalent widths. The source size is however highly uncertain in X-ray and such samples will not be used here.

- Flux-limited sample

  The sample needs to be flux-limited to properly account for amplification bias.

- The redshift and luminosity function

  The luminosity function from Boyle et al (2000) is based on the 2dF quasar sample and the LBQS sample in the redshift interval $0.35 < z < 2.3$. For quasar samples at higher redshift this luminosity function is not correct. There are indications that the bright end of the luminosity function shows a significant steepening with increasing redshift (Boyle et al, 2000). If a sample with very high redshift is used the uncertainty of the amplification bias will increase due to the uncertain luminosity function.

- Emission lines

  It is preferable to choose a low-ionized emission line because they are probably emitted from a BLR with larger radius than high-ionized emission lines. (If the BLR is to small then it can be magnified by small lenses.)

3.2 Quasar samples

3.2.1 Steidel & Sargent

The Steidel & Sargent sample (S&S, Steidel and Sargent, 1991, used by D94) was originally obtained for studying Mg II absorption line systems. It contains a very high signal-to-noise ratio spectra of 92 high-redshift quasars over the redshift range $0.7 \leqslant z \leqslant 2.7$. The equivalent widths of

CIII and MgII were originally measured to study the Baldwin effect. Candidates for the sample were initially selected from the Hewitt & Burbidge and Vèron-Cetty & Vèron catalogues to be bright and high in the northern sky (D94). The final number of measured equivalent widths is 87 of the 92 quasars in the sample.

The spectra were taken immediately after the quasars were selected, so this sample should be free of the reduction of amplification bias. The effective flux limit is $m_{B,limit} = 18.08$.

The sample is not complete.

Approximately two-thirds of the objects in the sample were selected by UV excess or radio power and should not be biased against small equivalent width quasars. The remaining objects were grism-selected and this could bias against small W_λ. To test this, the distribution of the grism-selected objects are tested with the Kolmogorov-Smirnov test (KS-test) and found to be statistically identical to the distribution for the UVX and radio-selected quasars.

For more details of the sample see Steidel and Sargent (1991).

The other sample used by D94 was the Einstein Medium Sensitivity Survey (EMSS, D94) but this sample will not be used here. The time delay between the photometry and spectroscopy for this sample was 2-5 years and this could affect the amplification bias with an unknown amount. In addition the equivalent widths were measured by hand from papercopies of the identification spectra, and it is X-ray selected.

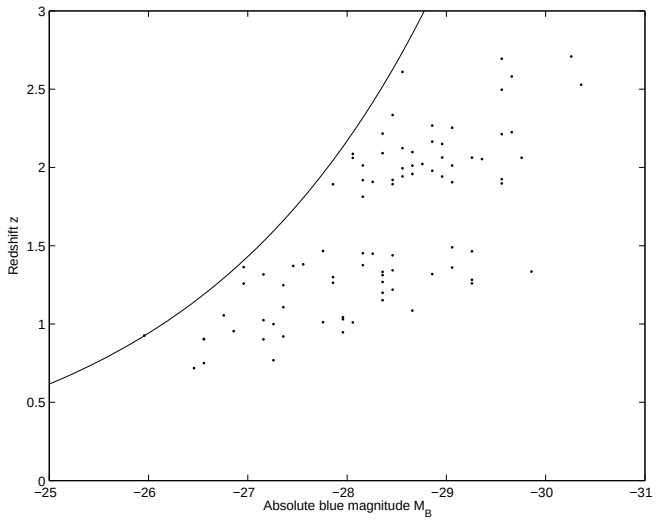

Figure 10: Absolute blue magnitude for the objects in the S&S sample are shown together with the effective flux limit, $m_B = 18.08$.

3.2.2 Large Bright Quasar Survey

Since the S&S sample is rather small and not complete other larger samples were searched for, as the Large Bright Quasar Survey (LBQS). This survey begun 1986 with the aim of identifying a homogeneous sample of 1000 bright quasars, $16 \leqslant m_{B_J} \leqslant 18.5$, over an extended redshift range, $0.2 \leqslant z \leqslant 3.4$. The spectroscopic phase of the project was essentially completed in 1989. LBQS is estimated to be $\approx 90\%$ complete (Hewett et al 1995, Forster et al 2001).

The LBQS sample have a combination of quantifiable selection techniques, including overall spectral shape, strong emission lines and redshifted absorption features. The LBQS thus avoids selection effects that tend to exclude weak-lined quasars or to undersample certain redshift ranges (Hewett et al 1995).

It is flux-limited with apparent magnitude $m_B = 18.85$. The flux limit of this sample will be below the magnitude at the break of the luminosity function (i.e. R will be less than 1) and the

amplification bias will be weak (see fig. 11). Constraints on this sample can only be found for high Ω_C and not for $\Omega_C = 0.10$ or 0.05 due to the weak amplification bias.

The other problem with this sample is the time delay between photometry and spectroscopy, which is 1-7 years. This affects the calculation of amplification bias with an unknown amount. Due to this uncertainty the LBQS sample cannot be used in this test.

If another lens model with a possibility to calculate the reduction of amplification bias was adopted, it would be possible to use this sample (see section 6.3).

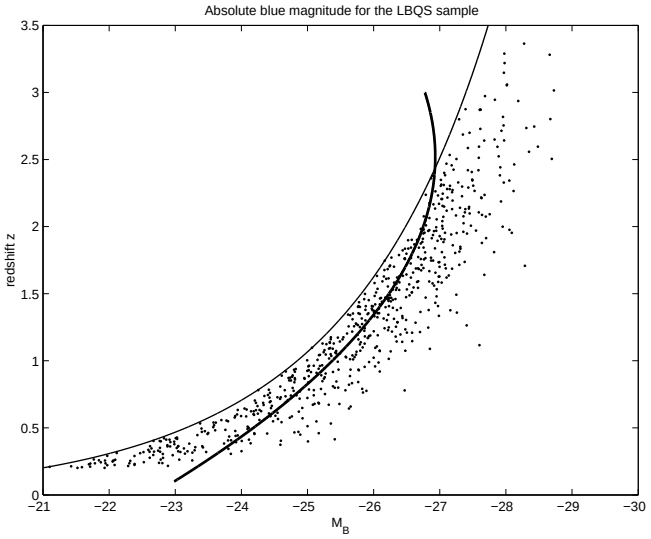

Figure 11: Absolute blue magnitude for the objects in the LBQS sample are shown together with the flux limit of the sample, $m_B = 18.85$ (thin solid) and the magnitude at the break of the luminosity function, M^* (thick solid).

4 Analysis

4.1 Properties and parameters for the Steidel & Sargent sample

From the S&S sample the measured CIII equivalent widths are used, but not the Mg II equivalent widths (D94 used both CIII and MgII). If a significant fraction of the apparent continuum is due to broad, low-contrast line emission as overlapping Fe II multiplets, this would affect this test on Mg II lines. Limits based on C III lines are unaffected.

The sample of CIII equivalent widths are divided into a high- and a low-redshift subsample. The properties for the CIII sample are listed in table 2.

The cumulative distributions of the subsamples are shown in fig. 12. Note the similarity in distributions. This already suggests that the amount of lensing by compact objects is small.

Table 2: Sample properties.

Sample	Redshift range	Number of objects	$< z >_{median}$	$< R >_{median}$
CIII S&S	$0.71 < z < 1.4$	40	1.18	1.31
	$1.4 \leqslant z < 2.71$	47	2.02	1.60

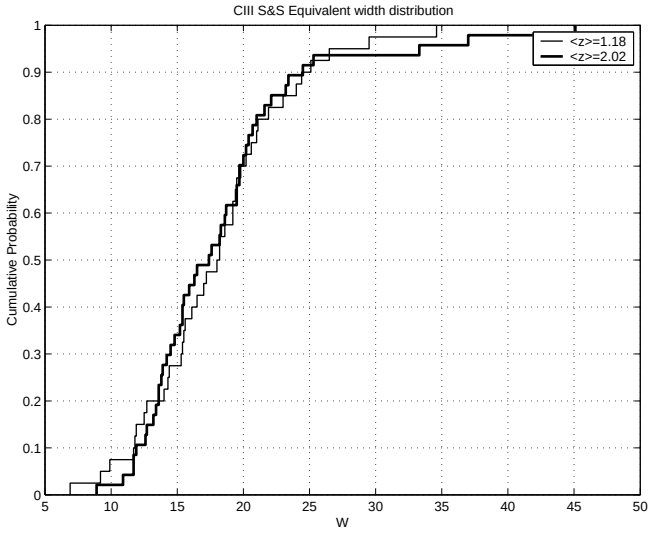

Figure 12: Equivalent widths for the subsamples of CIII S&S sample.

For the low-redshift subsample the parameters ω and γ for an underlying log normal distribution are chosen such that when lensed to the medium redshift of the low-redshift subsample, the model gave an acceptable fit to the data (the Kolmogorov-Smirnov test was used to show the probability of being the same distribution). Note that for different Ω_C new values of ω and γ are needed.

The parameters (γ and ω) for different Ω_C, the limiting equivalent width (W_{limit}), n_0 (the number of objects in the sample with $W < W_{limit}$) and the result of the KS-test is shown i table 3. W_{limit} is chosen such that the resulting Monte Carlo probability will be as low as possible.

To obtain a better fit for $\Omega_C = 0.3$ and 0.2, another function for the intrinsic distribution of equivalent widths ($p_0(W_0)$) needs to be found.

Table 3: Sample parameters.

Sample	W_{limit}	n_0	Ω_c	ω	γ	KS-test
CIII S&S	8.9 Å	0	0.30	0.2	2.9	0.17
			0.20	0.2	2.9	0.46
			0.10	0.22	2.9	0.91
			0.05	0.25	2.85	0.87

4.2 Comparison of data to model distribution

With these parameters (ω and γ) a model is generated for the high-redshift subsample, using the medium-redshift, W_{limit}, n_0 and $< R >$ for different Ω_C. The number of small equivalent width from the observations (n_0) are then compared to the number predicted by the model. A Monte Carlo test (based on 100,000 trials) is performed for different values of Ω_C and μ_{max} (corresponding to different values of the lens mass M_C). The resulting Monte Carlo probabilities are listed in table 5.

5 Results

5.1 Comparison between Einstein-de Sitter cosmology and a Λ-dominated Universe

The resulting models for an Einstein-de Sitter and a Λ-dominated cosmology is shown in fig. 13 together with the distribution of the high redshift subsample of the S&S CIII. All parameters in the models are the same except for Ω_M and Ω_Λ; $\Omega_C = 0.3$ in both models. Due to the increased path length the new optical depth has increased compared to an Einstein-de Sitter universe (fig. 2). This *increases* the probability of lensing for the same Ω_C and *decreases* the resulting Monte Carlo probability (i.e. the constraints on Ω_C will be *stronger*).

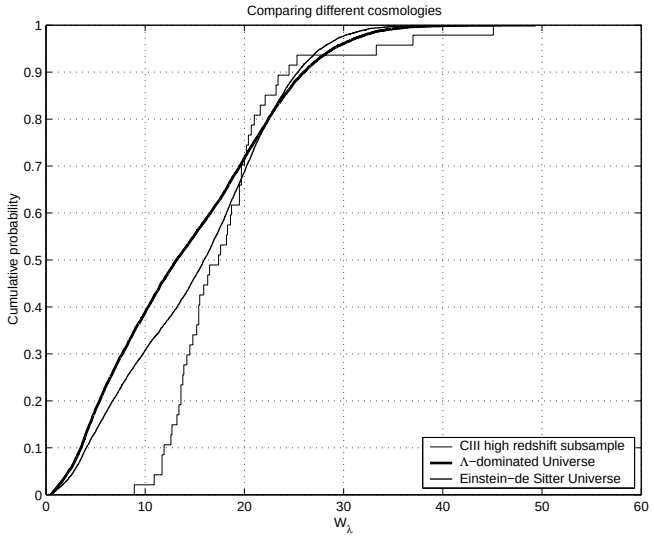

Figure 13: The distribution of the high-redshift subsample of CIII from the S&S sample is shown together with models with different cosmologies for $\Omega_C = 0.3$. $\Omega_M = 0.3$ and $\Omega_\Lambda = 0.7$ (thick solid). $\Omega_M = \Omega_C = 0.3$, $\Omega_\Lambda = 0$ (thin solid). All other parameters are the same: $\alpha = 3.41$, $\beta = 1.58$, $\gamma = 0.2$, $\omega = 2.9$, R=1.6, $\mu_{max} = 6.2$ and z=2.02.

5.2 Amplification bias

In addition to different cosmologies, different luminosity functions and the strength of the amplification bias can be compared. The strongest impact on the amplification bias here is the fact that the new slope of the luminosity function is less steep ($\alpha = 3.41$, $\beta = 1.58$ compared to $\alpha = 3.97$, $\beta = 1.41$). In addition the strength of amplification bias has decreased. In D94 $< R >= 2.164$ for the S&S CIII high-redshift subsample, here $< R >= 1.60$. The resulting effect is that the probability of lensing has *decreased* for the S&S sample and *weaker* constraints on Ω_C can be set if this sample is used. This is shown in fig. 14 with $\Omega_C = 0.3$ and in fig. 15 with $\Omega_C = 0.05$. The two different models in each figure have different cosmologies, different luminosity functions and different $< R >$. The difference between the two cosmologies in the model distributions decreases with Ω_C. Another brighter sample is needed to maintain the same amplification bias as in D94 and make the constraints on Ω_C stronger than in D94.

The effect of the amplification bias is very strong. In fig. 16, models with and without the amplification bias is shown for a Λ-dominated cosmology. With an apparent magnitude $m_B = 18.85$ for the LBQS sample, $< R >= 0.77$ for the high-redshift subsample. To show the difference in strength of the amplification bias a model with $< R >= 1.2$ is also shown. To obtain a correct Monte Carlo probability it is very important to have a correct calculated amplification bias.

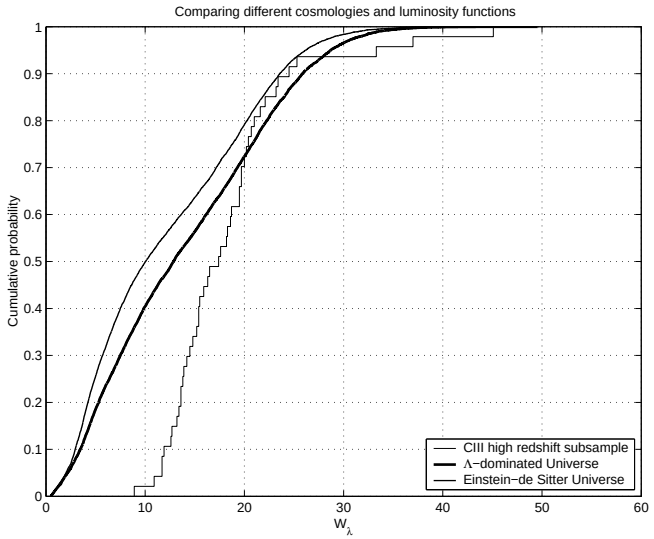

Figure 14: The distribution of the high-redshift subsample of CIII from the S&S sample is shown together with models with different cosmologies, different luminosity functions and amplification bias for $\Omega_C = 0.3$. $\Omega_M = 0.3$, $\Omega_\Lambda = 0.7$,$\alpha = 3.41$, $\beta = 1.58$ and R=1.60 (thick solid). $\Omega_M = 0.30$, $\Omega_\Lambda = 0$, $\alpha = 3.97$, $\beta = 1.41$, R=2.164 (thin solid). For both models: $\gamma = 0.2$, $\omega = 2.9$, z=2.02 and $\mu_{max} = 6.2$.

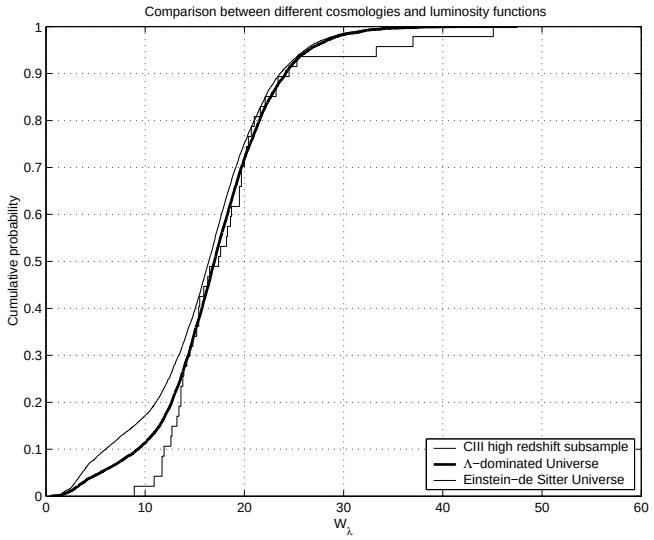

Figure 15: The distribution of the high-redshift subsample of CIII from the S&S sample is shown together with models with different cosmologies, different luminosity functions and amplification bias for $\Omega_C = 0.05$. $\Omega_M = 0.3$, $\Omega_\Lambda = 0.7$, $\alpha = 3.41$, $\beta = 1.58$ and R=1.60 (thick solid). $\Omega_M = 0.05$, $\Omega_\Lambda = 0$, $\alpha = 3.97$, $\beta = 1.41$, R=2.164 (thin solid). For both models: $\gamma = 0.2$, $\omega = 2.9$, z=2.02 and $\mu_{max} = 6.2$.

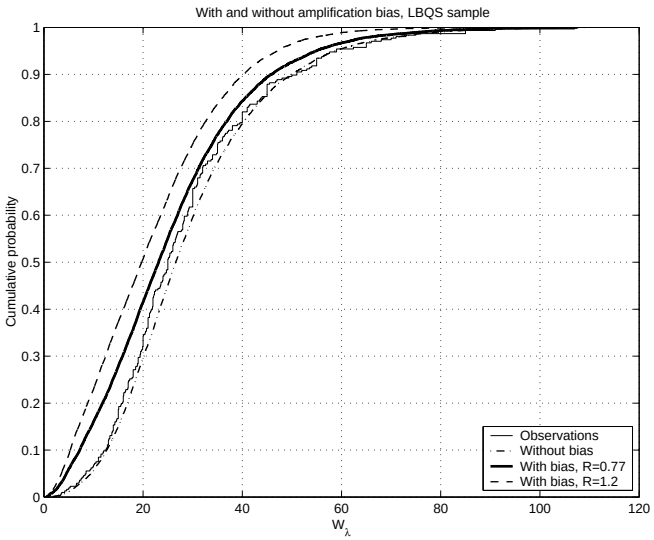

Figure 16: The distribution of the high-redshift subsample of CIII from the LBQS sample is shown together with models for a Λ-dominated Universe and with a new luminosity function, $\Omega_M = \Omega_C = 0.3$, $\Omega_\Lambda = 0.7$, $\alpha = 3.41$, $\beta = 1.58$, $\mu_{max} = 6.2$, z=1.95. Without amplification bias, $\gamma = 0.45$, $\omega = 3.15$ (dash-dotted). With amplification bias: R=0.77, $\gamma = 0.42$, $\omega = 3.2$ (thick solid); R=1.2, $\gamma = 0.35$, $\omega = 3.3$ (dashed).

5.3 Upper mass limits on compact objects

In D94 the allowed $\Delta f/f \leqslant 0.25, 0.50, 0.75$ for $\Omega_C = 0.1$, 0.2, 1 . This corresponds to upper mass limits of $M_C = 20$, 60 and $300\,M_\odot$ with the assumption of a BLR size of 0.1 pc ($= 3.0857 \cdot 10^{15}$ m).

Since the BLR size could be as small as 10^{15} m (Kaspi et al, 2000) this affect the upper mass limits. With this BLR size the upper mass limits in D94 are lowered to $M_C = 2$, 8 and $40\,M_\odot$.

Here $\Delta f/f$ is allowed to be $\leqslant 0.15$, 0.25, 0.50, 0.75 for $\Omega_C = 0.05$, 0.10, 0.20 and 0.30 respectively. The corresponding upper limits on lens masses are 1, 2, 8 and $40\,M_\odot$. If the allowed $\Delta f/f$ is lowered then the upper limits of the lens masses decreases. In table 4 the corresponding $\Delta f/f$, μ_{max} and lens masses are listed for a BLR size of 10^{15} m calculated with the approximation (44). If the allowed $\Delta f/f$ is changed, new upper mass limits can be found here.

Note that these approximative values can be compared with a more correct calculation from (43), but then μ_{limit} is approximative. With $\mu_{limit} = 2$ the resulting $\Delta f/f$ from (44) is approximately equal with (43) for $\Omega_C = 0.3$, but for lower values of Ω_C $\Delta f/f$ from (43) increases compared to $\Delta f/f$ from (44) for the same μ_{BLR}. Thus the upper limits on lens masses are not the same for different Ω_C (decreases with Ω_C).

No constraints can be derived for lens masses over these upper limits. Note that if $\Delta f/f$ is only allowed to be ≈ 0.10 for $\Omega_C = 0.05$ then the upper mass limit is lowered to $\approx 0.6\,M_\odot$.

Fig. 17 show the dependence of μ_{max} of the lens mass for different BLR sizes.

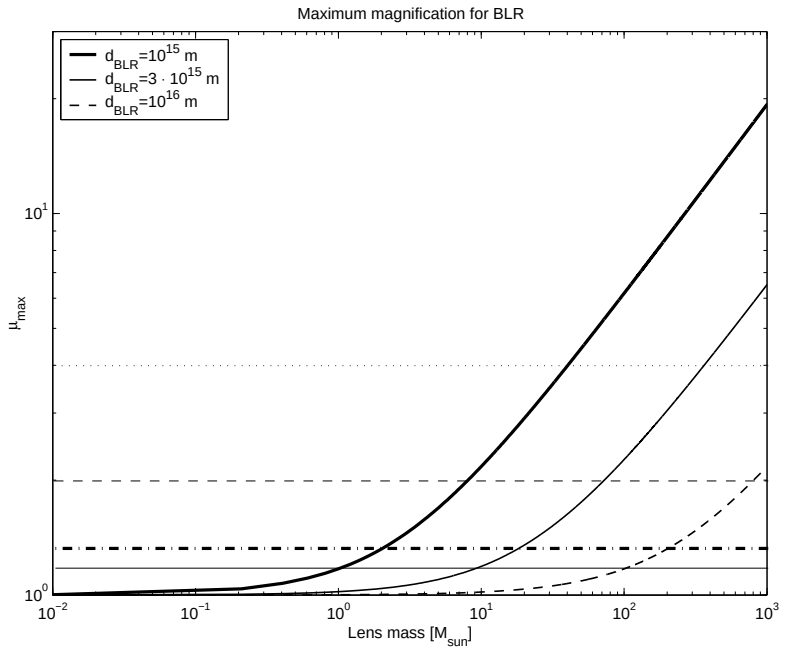

Figure 17: Maximum magnification as a function of lens mass for different BLR sizes; $d_{BLR} = 10^{15}$ m (thick solid), $d_{BLR} = 3 \cdot 10^{15}$ m (thin solid), $d_{BLR} = 10^{16}$m (dashed). The horizontal lines indicate the maximum magnification for which lensing of the BLR would reduce the fraction of weak-lined objects by 15% ($\mu_{max} = 1.18$, thin solid), 25% ($\mu_{max} = 1.33$, dash-dotted), 50% ($\mu_{max} = 2$, dashed) and 75% ($\mu_{max} = 4$, dotted).

Table 4: Upper mass limits.

$\Delta f/f$	μ_{BLR}	M_C $[M_\odot]$
0.10	1.11	0.6
0.15	1.18	1.0
0.20	1.25	1.5
0.25	1.33	2.1
0.30	1.43	2.8
0.35	1.54	3.7
0.40	1.67	4.8
0.45	1.82	6.2
0.50	2.0	8.1
0.55	2.22	11
0.60	2.5	14
0.65	2.9	19
0.70	3.33	27
0.75	4.0	40

5.4 Lower mass limits on compact objects

The lowest lens mass this test can constrain depends on the source size, Ω_C, the redshift of the sample (through the optical depth) and the total number of objects in the high-redshift subsample.

In table 1 the corresponding lens masses, source sizes and μ_{max} are listed. For very low μ_{max} no constraints can be obtained for these lens masses because the lenses are to small to take the object into the small equivalent region. If $\mu_{max} = 1.2$ then the resulting Monte Carlo probabilities are ~ 1 thus $\mu_{max} = 1.2$ is not listed in the resulting table 5. The lowest lens mass this test can constrain therefore corresponds to $\mu_{max} = 2.17$.

Another argument against using very small μ_{max} is the fact that the lens model is not correct in the small magnification region (see section 2.6).

5.5 Constraints on Ω_C

The resulting Monte Carlo probabilities for finding the observed number of weak-lined objects are listed in table 5. Based on these probabilities Ω_C is constrained for different source sizes (fig. 18) with max $p(n < n_0) = 0.02$. With the assumption of a source size equal or less than 10^{13} m the constraints of D94 are improved: $\Omega_C < 0.05$ for $M_C = 0.01 - 1\, M_\odot$, $\Omega_C < 0.1$ for $M_C = 0.01 - 2\, M_\odot$, $\Omega_C < 0.2$ for $M_C = 0.001 - 8\, M_\odot$ and $\Omega_C < 0.3$ for $M_C = 0.001 - 40\, M_\odot$.

For small source sizes the Monte Carlo probabilities are only calculated for very small lenses, because for high μ_{max} the probabilities will be the same (see section 2.10). For $l_s = 10^{12}$ m, Ω_C is thus < 0.05 for lenses in the mass range 10^{-4} to $1 M_\odot$ even if the probabilities were only calculated up to $M_C = 0.01\, M_\odot$.

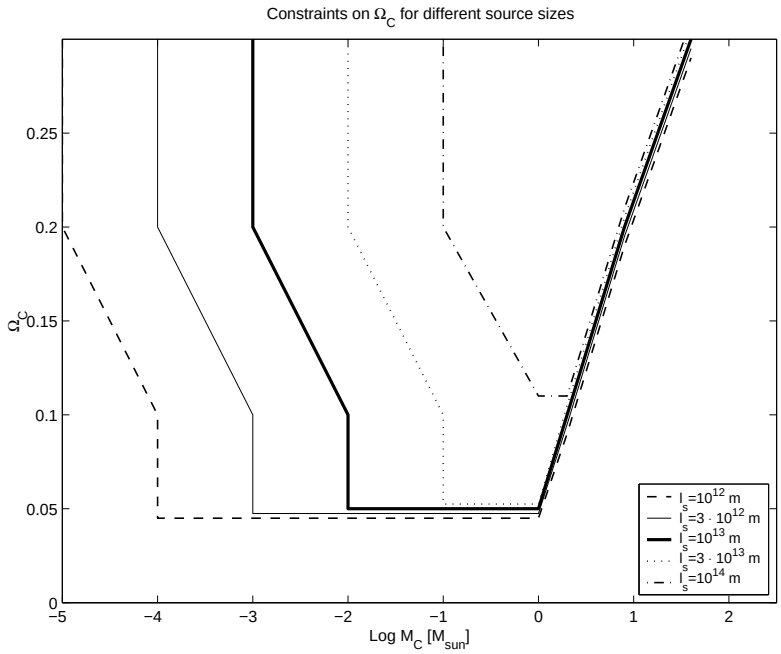

Figure 18: Upper limits on Ω_C for differents source sizes and lens masses inferred from the resulting Monte Carlo probabilities.

Table 5: Monte Carlo results for CIII S&S sample.

Ω_c	μ_{max}	10^{12}m M_C $[M_\odot]$	$3 \cdot 10^{12}$m M_C $[M_\odot]$	10^{13}m M_C $[M_\odot]$	$3 \cdot 10^{13}$m M_C $[M_\odot]$	10^{14} m M_C $[M_\odot]$	$P(n \leqslant n_0)$
0.30	2.17	10^{-5}		10^{-3}		0.1	0.00006
	2.27		10^{-4}		0.01		$< 10^{-5}$
	6.18	10^{-4}		10^{-2}		1	$< 10^{-5}$
	6.51		10^{-3}		0.1		$< 10^{-5}$
	19.32	10^{-3}		0.1		10	$< 10^{-5}$
	20.36		10^{-2}		1		$< 10^{-5}$
	61	0.01		1			$< 10^{-5}$
	64		0.1		10		$< 10^{-5}$
0.20	2.17	10^{-5}		10^{-3}		0.1	0.00129
	2.27		10^{-4}		0.01		0.00087
	6.18	10^{-4}		10^{-2}		1	$< 10^{-5}$
	6.51		10^{-3}		0.1		$< 10^{-5}$
	19.32	10^{-3}		0.1		10	$< 10^{-5}$
	20.36		10^{-2}		1		$< 10^{-5}$
	61	0.01		1			$< 10^{-5}$
	64		0.1		10		$< 10^{-5}$
0.10	2.17	10^{-5}		10^{-3}		0.1	0.05372
	2.27		10^{-4}		0.01		0.03994
	6.18	10^{-4}		10^{-2}		1	0.00060
	6.51		10^{-3}		0.1		0.00032
	19.32	10^{-3}		0.1			0.00017
	20.36		10^{-2}		1		0.00016
	61	0.01		1			0.00015
	64		0.1				0.00014
0.05	2.17	10^{-5}		10^{-3}		0.1	0.19135
	2.27		10^{-4}		0.01		0.16569
	6.18	10^{-4}		10^{-2}		1	0.01585
	6.51		10^{-3}		0.1		0.01535
	19.32	10^{-3}		0.1			0.00798
	20.36		10^{-2}		1		0.00786
	61	0.01		1			0.00733
	64		0.1				

6 Discussion

6.1 Comparison with the constraints on Ω_C from D94

The constraints calculated here are even stronger when compared to D94, except for the upper mass limits that have decreased due to a smaller BLR size.

How is this possible if a weaker amplification bias for the S&S sample has reduced the probability of lensing (even with the increased optical depth from a Λ-dominated Universe)? The reason for this is that D94 did not use the correct luminosity function for the S&S sample! The luminosity function intended only for the EMSS sample (from Maccacaro et al 1991, with $\alpha = 3.05$, $\beta = 1.35$) were also used for the S&S sample where the luminosity function from Boyle (1990) should have been used (with $\alpha = 3.97$, $\beta = 1.41$). Their Monte Carlo results for the S&S sample are thus not correct and should have been much lower for this sample and their constraints on Ω_C could have been much stronger!

Here the the delta function for $p_2(\mu_u)$ at the cutoff is added at $\mu_u = \mu_{max}^2$ and not as in D94 at $\mu_u = \mu_{max}$. The argument for this is that if the minimum magnification for $p_2(\mu_u)$ is μ_0^2, the maximum magnification should be $\mu_u = \mu_{max}^2$. In addition the resulting Monte Carlo probabilities for low μ_{max} and the figures here with the calculated models for different μ_{max} (with an Einstein-de Sitter cosmology) only agrees with D94 if the delta function is added at $\mu_u = \mu_{max}^2$. The conclusion is that the cutoff for $p_2(\mu_u)$ should be placed at $\mu_u = \mu_{max}^2$ and that this probably is another misprint in D94.

6.2 Possible uncertainties

The resulting constraints on Ω_C is dependent on a number of things:

The S&S sample is not complete. This could affect the distribution of equivalent widths and the obtained constraints on Ω_C.

The amplification bias needs to be correct calculated. This is dependent on a correct luminosity function (α, β and M^*) and a correct calculated $< R >_{median}$.

The upper mass limits are uncertain due to the fact that $\Delta f/f$ is arbitrary chosen.

The lensing model is approximative but conservative because it tends to underestimate the true amount of lensing.

If the standard model of quasar structure is not correct as suggested by Schild and Vakulik (2003) the lensing model needs to be adjusted. In their model a luminous inner accretion disc edge and outer ring-shaped structures where the emissions lines form are suggested. This would affect the magnification signature of the microlensing event.

The cosmological evolution of the intrinsic distribution of equivalent widths cannot explain the small number of equivalent widths objects. The evolutionary trend is in fact towards smaller equivalent widths at higher redshift, which is the opposite to what is needed to mask microlensing (D94).

Finally, there is a possibility of bugs in my matlab codes. To check my codes I reproduced all the Monte Carlo probabilities and every figure in D94 (the optical depth, maximum magnification, the model distributions for both the EMSS and S&S samples) and they all agreed (with an Einstein-de Sitter cosmology), except for the final models of the S&S sample. If the luminosity function from the EMSS sample was used instead for this sample, then these figures and Monte Carlo probabilities agreed too.

6.3 Continuing this work

The results in this work can be improved by using a better sample with many objects at high redshift, with high amplification bias and where the time delay between the selection of quasars and spectroscopy is short.

It would also be interesting to test another lens model from Zackrisson and Bergvall (2002) to see if even stronger constraints can be inferred. A more correct calculation of the upper mass

limits can also be done with this lens model. The reduced amplification bias in the LBQS sample may be calculated and then this sample can be used.

6.4 The future of microlensing in the search for dark matter

Cluster-cluster microlensing will be used by Tomonori Totani (2002) in an attempt to set limits on intracluster compact objects for a very wide range of lens masses ($10^{-5} - 10^{10}\ M_{\odot}$). Two clusters which are almost in perfect alignment, A2152 (in the Hercules supercluster) at z=0.04 and another just behind it at z=0.13 will act as source and lens. With a deep and wide monitoring of the region with the 8 m Subaru/Suprime-Cam telescope, extremely magnified stars in the background cluster by microlensing of compact objects in A2152 may be detectable. This method is very powerful. Any compact object in this mass range can be detected or rejected as a dominant component of dark matter. The observations have already begun and will continue in June, 2003.

There is another form of microlensing called astrometric microlensing, and is caused by nearby lenses. This form of microlensing has not been observed yet, but it will be within the next decade by one of the microsecond astrometric satellites, SIM (Space Interferometry Mission) or GAIA. If a microlensing event with a nearby lens is monitored by GAIA and the Einstein crossing time, the relative parallax of the source with respect to lens can be inferred from GAIA, and the source distance is known, then a complete solution of the microlensing parameters is available (Evans, 2003).

Other galaxies as M33 are also interesting targets for dark matter studies with microlensing (Evans, 2003). This galaxy is a low luminosity spiral galaxy in the Local Group. The dark matter content of low luminosity and dwarf galaxies are different from big bright galaxies. In M33 it is clear that the dark matter must dominate even the central parts, in contrast to the Milky Way which is dominated by luminous matter within the inner few kpc. The MACHO and EROS projects have demonstrated that substellar compact objects are not the dominant contributor to the Milky Way's dark halo. But this conclusion cannot be extended to galaxies like M33 without further experiments.

7 Summary

The upper limits on the cosmological density of compact objects has been improved compared to that of D94 by:

Generalizing from an Einstein-de Sitter Universe to a Λ-dominated Universe with $\Omega_M = 0.3$ and $\Omega_\Lambda = 0.7$. A new optical depth is derived and calculated with the new cosmology. Due to the increased path length the optical depth is increased and therefore the constraints on Ω_C will be stronger with a Λ-dominated cosmology.

The situation when $\Omega_C \neq \Omega_M$ is solved and different values of Ω_C with constant $\Omega_M = 0.3$ is calculated.

A new luminosity function (Boyle, 2000) is adopted and new strengths of the amplification bias are found. This decreases the amplification bias for the sample used here and by D94 (the constraints are weaker for this sample).

Uncertainties of the source size are considered. This decides the maximum magnification of the source for different lens masses and determines the lower mass limits in this test. The source size is found to correlate with lens mass for a constant magnification. If the CR is large then only high mass lenses can be constrained, whereas small CR sizes can constrain very small lenses.

Smaller sizes of the broad line region are taken into account. This lowers the upper lens masses that can be constrained by this test. Due to the arbitrary choice of the allowed value of the reduction of small equivalent width objects these upper mass limits is uncertain.

New improved constraints on Ω_C have been calculated using the same sample as by D94. With the assumption of a source size equal or less than 10^{13} m the constraints of D94 are improved: $\Omega_C < 0.05$ for $M_C = 0.01-1 M_\odot$, $\Omega_C < 0.1$ for $M_C = 0.01-2 M_\odot$, $\Omega_C < 0.2$ for $M_C = 0.001-8 M_\odot$ and $\Omega_C < 0.3$ for $M_C = 0.001 - 40\, M_\odot$.

All these issues have been examined by implementing the D94 method in matlab.

8 Acknowledgements

I would like to thank my supervisor Erik Zackrisson for his support and encouragement. Thank you for your time, for your advice and for listening to all my questions and ideas.

9 Appendix A

1. **MC_result_grid.m** This code calculates the resulting Monte Carlo probability for a given Ω_C with different μ_{max}.

   Subroutines:

   - **prob_dist.m**
     This function calculates the emission line equivalent width distribution (equation 47).
     Subroutines:
     - **optical_depth.m**
       Calculates the new optical depth (equation 28).
       Subroutine:
       * **lambda_new.m**
         Calculates the new affine parameter (equation 10).
     - **p1_total_old.m** Calculates the total p_1 to $\mu = 5003$. Needed for the delta function added at μ_{max}.
     - **p2_total_old.m** Calculates the total p_2 to $\mu = 5003$. Needed for the delta function added at μ^2_{max}.
     - **P0W0.m** A function which calculates the unlensed equivalent width distribution (equation 48).
   - **MonteC_grid.m**
     This function Monte Carlo simulates 47 (the total number of objects in the high redshift subsample) equivalent widths for the model probability distribution.

2. **tao_new.m** Calculates and plots the optical depth as a function of redshift (equation 28 and fig. 2)

   Subroutines:

   - **optical_depth.m**
     Subroutine:
     - **lambda_new.m**

3. **mymax.m** Calculates and plot the maximum magnification as a function of lens mass for a specific source size (equation 31 and 32)

   Subroutine:

   - **optical_depth.m**
     Subroutine:
     - **lambda_new.m**

4. **R_median.m** Calculates $< R >_{median}$ for a specific apparent magnitude and $< z >_{median}$.

   Subroutine:

   - **angsiz.m**
     Calculates the integral for the angular size.

5. **absmag.m** Calculates and plot the absolute magnitudes of the objects in the LBQS sample together with the flux limit of the sample and magnitude at the break of the luminosity function.

   Subroutine:

- **CIII_LBQS**
  A file with the apparent magnitudes, redshifts and equivalents widths for the objects in the S&S sample.
- **angsiz.m**

6. **absmag_SS.m** Calculates and plot the absolute magnitudes of the objects in the S&S sample together with the flux limit of the sample.

   Subroutines:

   - **angsiz.m**
   - **CIII_alla** A file with the absolute magnitudes, redshifts and equivalents widths for the objects.

7. **cum_obs.m** Plots the cumulative probability for the S&S sample (or LBQS sample) for the low or high redshift subsample.

   Subroutine:

   - **CIII_alla**

8. **MonteCarlo.m** Monte Carlo simulation and plotting of 10,000 equivalent widths from equation 47.

   Subroutine:

   - **prob_dist.m**

References

[1] Abajas, C., et al, ApJ, 576, 640, 2002.

[2] Afonso, C., et al, astro-ph/0212176, 2003.

[3] Alcock, C., et al, ApJ, 542, 281, 2000.

[4] Bartlemann, M., Schneider, P., AA, 239, 113, 1990.

[5] Boyle, B., J., MNRAS, 243, 1, 1990.

[6] Boyle, B., J., et al, MNRAS, 317, 1014, 2000.

[7] Canizares, Claude, R., ApJ, 263, 508, 1982.

[8] Carr, B., J., astro-ph/0008028, 2000.

[9] Coles, P., Lucchin, F., England, Cosmology. The Origin and Evolution of Cosmic Structure, 2002.

[10] Collin, S., Huré, J., M., AA, 372, 50, 2001.

[11] Dalcanton, Julianne, J., Canizares, Claude, R., Granados, Arno, Steidel, Charles, C., Stocke, John, T., ApJ, 424, 550, 1994.

[12] Dyer, C., C., Roeder, R., C., AJ, 174, L115, 1972.

[13] Evans, N., W., astro-ph/0304252, 2003.

[14] Forster, K. et al, ApJS, 134, 35, 2001.

[15] Hewett, P.C., Foltz, C.B., Chaffee, F.H., AJ, 109, 1498H, 1995.

[16] Kailash, C., Sahn, astro-ph/0302325, 2003.

[17] Kaspi, S., et al, ApJ, 533, 631, 2000.

[18] Kayser, R. et al, AA, 318, 680, 1997.

[19] Peacock, J., A., MNRAS, 199, 987, 1982.

[20] Press, W., Gunn, J., ApJ, 185, 397, 1973.

[21] Refsdal, S., et al, AA, 360, 10, 2000.

[22] Schild, R., Vakulik, V., astro-ph/0303356, 2003.

[23] Schneider, P., AA, 179, 80, 1987.

[24] Schneider, P., Ehlers, J., Falco, E., Gravitational Lensing, Springer verlag, Berlin, 1991.

[25] Schneider, P., AA, 254, 14, 1992.

[26] Schneider, P., MNRAS, 292, 673, 1997.

[27] Seitz, S., Schneider, P., Ehlers, J., astro-ph/9403056, 1994.

[28] Shalyapin, V.N., et al, astro-ph/0207236, 2002.

[29] Spergel, D. N. et al, astro-ph/0302209, 2003.

[30] Steidel, C. C., Sargent, W., L., W., ApJ, 382, 433, 1991.

[31] Tomonori Totani, ApJ, 586, 735, 2002.

[32] Walker, M., Wardle, M., PASA, 16, 262, 1999.

[33] Wambsganss, J., ASP Conference Series, vol 239, 2000.

[34] Wambsganss, J., astro-ph/0207616, 2002.

[35] Wandel, A., et al, ApJ, 526, 579, 1999.

[36] Weinberg, S., ApJ, 208, L1, 1976.

[37] Wyithe, J., S., B., et al, MNRAS, 315, 62, 2000.

[38] Wyithe, J., Turner, E., ApJ, 575, 650, 2002.

[39] Zackrisson, E., Bergvall, N., AA, 399, 23, 2003.